FIBRE LOCK-UP AND OTHER MECHANISMS AT LARGE FIBRE ROTATIONS, AND THEIR EFFECT ON AXIAL COMPRESSION OF COMPOSITES

Robin Olsson[1]

[1]Swerea SICOMP, Box 104, SE-431 22 Mölndal, Sweden
Email: robin.olsson@swerea.se, Web Page: http://www.swerea.se/en/sicomp

Keywords: fibre kinking, lock-up, 3D fibre array

Abstract
This paper studies the sequence of fibre kinking, the fibre lock-up and the subsequent constitutive behaviour. The conditions governing these phenomena are discussed with focus on the conditions for fibre lock-up. Lower bounds for the fibre lock-up angle α and the kink band angle β are derived purely from geometrical conditions for 3D arrays of fibres, with the aim to define the termination of fibre kinking in homogenized material models for FE analysis. It is concluded that the limit of the lock-up angle is 90° for low fibre volume fractions, decreases to about 50° for fibre volume fractions common in high performance composites, and reaches zero for fully packed fibres.

1. Introduction

Fibre rotation is a key mechanism in axial compressive failure of fibre composites, which eventually results in "fibre kinking" [1-7]. Compressive shear failure of the fibres sometimes precedes kinking, particularly for stiff matrices, but this normally triggers kinking of neighbouring fibres [7]. Ultimately, large rotations cause fibre lock-up due to geometrical constraints or matrix strain hardening, Fig. 1.

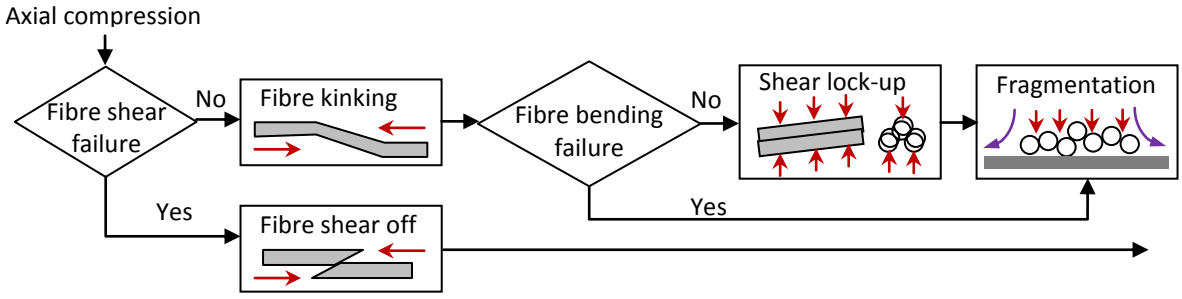

Figure 1. Failure sequence for fibre compression.

A recent model for fibre kinking incorporates shear softening due to initiation and growth of shear micro-cracks [8-9]. The stresses resulting from friction on the crack surfaces increase linearly with the damage variable, and remain at a constant and non-negligible level after fully developed damage. Hence, these stresses should be accounted for until final fibre lock-up.

The damage initiation and peak stress ("compressive strength") typically occur at small fibre rotations, but the conditions and behaviour at large fibre rotations are essential for the energy absorption during in-plane crushing, e.g. for correct simulation of car crash events. The fibre lock-up angle α is crucial,

as it terminates the fibre rotation process, and initiates a different constitutive behaviour, with higher stiffness resulting in kink band broadening, i.e. fibre kinking in the surrounding material. In FE-simulations element deletion prior to fibre lock-up may result in severe underestimation of the energy consumed during crash events.

The available analytical models for fibre kinking are based on a 2D micromechanics analysis, i.e. the fibres and matrix are considered as slabs in a layered continuum. Most analytical models have assumed that the fibre lock-up angle α is given by $\alpha \approx 2\beta$, where β is the kink-band angle. An overview of experimentally observed values of β was given in [2]. Recently, however, two analytical models derived explicit relations between β and α. Zidek and Völlmecke [5] obtained solutions for α substantially smaller than 2β, while Skovsgaard and Myhre Jensen [6] obtained values of α slightly larger than 2β, by noting when the strain energy exceeded the applied work for further deformation. A major limitation of the analytical models is the 2D analysis which disregards the 3D nature of fibres in the composite. Furthermore, matrix cracking and friction are neglected.

The 3D nature of the micromechanics problem has been considered in some FE analyses [10-12]. The analysis in [10] was focused on initiation of kinking, while the studies [11-12] considered some further development although none of the simulations was pursued to fibre lock-up, probably due to computational problems at large strains.

Some previous studies, e.g. [2, 7], have included in-situ 2D microscopy of the kinking process, including the increasing fibre rotation, kink band angle and fibre lock-up angle. A limitation of these studies is obviously that only the angular component in the plane of microscopy is measured, while the total angle may be larger. This limitation was avoided in a recent study using 3D micro-computed tomography of fibre kinking [13]. The study documented kink band angles β of 11°-40° and fibre rotations $\theta \leq \alpha$ of up to 52°, which is significantly larger than the angles noticed in 2D microscopy but still may be an underestimation of α as the specimens were scanned after unloading.

The current paper derives bounds for the kink-band angle β and fibre lock-up angle α for 3D fibre configurations purely from geometrical considerations. These bounds may be used to determine the ultimate shear strain in homogenized kinking models of the type presented in [8-9].

2. Volumetric considerations

The relation between the fibre lockup angle α, or more generally the fibre rotation, and the kink band angle β may be defined from purely volumetric considerations, Fig. 2. This observation was made already in [1], but is re-derived here for purpose of clarity.

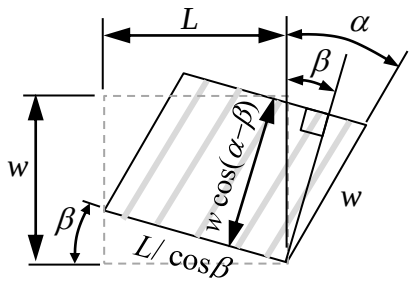

Figure 2. Definition of kinking geometry

Fibres in typical fibre reinforced composites are very stiff in comparison to the matrix, and may be approximated as inextensible. Assuming plane strain in this case for a slab of thickness h the volumes V_0 in the undeformed position and V_1 in the deformed position at fibre lockup are then given by:

$$V_0 = hwL \qquad V_1 = hw\cos(\alpha-\beta)L/\cos\beta \tag{1}$$

Considering volumetric relations we get the following expressions:

$$\text{Incompressible material: } V_1 = V_0 \Rightarrow \cos(\alpha-\beta)/\cos\beta = 1 \Rightarrow \alpha = 2\beta \tag{2a}$$

$$\text{Compressible material: } V_1 < V_0 \Rightarrow \cos(\alpha-\beta)/\cos\beta < 1 \Rightarrow \alpha > 2\beta \tag{2b}$$

Lock-up typically occurs at relatively large shear strains (large values of α), well beyond the elastic range of the matrix. In cases where the matrix deformation involves matrix shear cracking [8-9] or approaches an ideally plastic behaviour the material approaches the incompressible case, i.e. $\beta \rightarrow \alpha/2$.

3. Conditions for fibre lock-up

3.1. Lock-up with locking fibres in parallel planes

We will consider the geometric conditions for fibre lock-up for the 2D case with layered slabs, the 3D case with fibres in a square array and fibres in a hexagonal array. The geometric conditions for fibre lock-up are the same for the 2D case (2D), the 3D square array (Sq) and the hexagonal array with a horizontal symmetry axis (HxH), Fig. 3. Note that the 2D case assumes an unphysical compression of the matrix to zero volume at fibre lock-up.

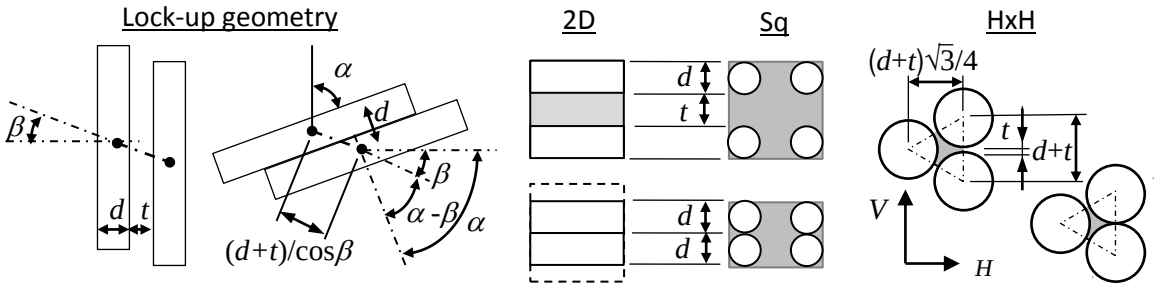

Figure 3. Lock-up geometry and geometries for 2D, 3D Sq and 3D HxH fibre arrays.

For all the cases in Fig. 3 the lock-up geometry is characterised by the following equations:

$$\begin{aligned} d = \cos(\alpha-\beta)\cdot(d+t)/\cos\beta \quad &\Rightarrow \quad \cos(\alpha-\beta) = C\cos\beta \\ \alpha = \beta + \text{Arccos}(C\cos\beta) \quad &\text{where} \quad C = d/(d+t) \end{aligned} \tag{3}$$

where C is a function of the fibre volume fraction, specific for each fibre array. The fibre volume fraction and $C = d/(d+t)$ for the different cases are given by:

$$\text{2D:} \qquad v_f = d/(d+t) \qquad \Rightarrow \qquad C = v_f \tag{4}$$

$$\text{Sq:} \qquad v_f = \frac{\pi d^2}{4(d+t)^2} \le \pi/4 \approx 0.785 \qquad \Rightarrow \qquad C = \sqrt{v_f\, 4/\pi} \tag{5}$$

$$\text{HxH:} \qquad v_f = \frac{\pi d^2}{2\sqrt{3}(d+t)^2} \le \frac{\pi}{2\sqrt{3}} \approx 0.907 \quad \Rightarrow C = \sqrt{v_f 2\sqrt{3}/\pi} \tag{6}$$

3.2. Lock-up with locking fibres in intersecting planes

For fibres in a hexagonal array with vertical symmetry axis (HxV) the geometry is given by Fig. 4.

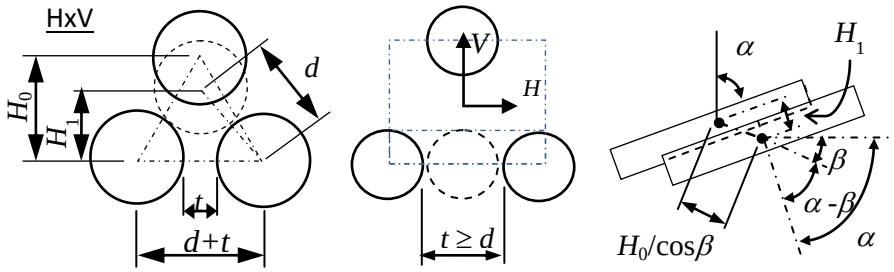

Figure 4. Lock-up geometry and geometry for HxV fibre array.

The fibre volume fraction for HxV is equal to that for HxH as given by Eq. (6). The geometrical quantities H_0 (original height of triangle) and H_1 (height of triangle at fibre lock-up) are given by:

$$H_0 = (d+t)\sqrt{3}/2 \qquad H_1 = \sqrt{d^2 - (d+t)^2/4} \tag{7}$$

The quantities H_0 and H_1 may be defined from the fibre volume fraction v_f as follows:

$$v_f = \frac{\pi d^2}{2(d+t)^2\sqrt{3}} \le \frac{\pi}{2\sqrt{3}} \approx 0.907 \qquad d/(d+t) = \sqrt{v_f 2\sqrt{3}/\pi}$$

$$v_f \le \frac{\pi}{8\sqrt{3}} \approx 0.227\ (t \ge d) \Rightarrow\ H_1 = 0 \qquad v_f > \frac{\pi}{8\sqrt{3}} \Rightarrow \quad H_1/H_0 = \sqrt{\frac{8v_f}{\pi\sqrt{3}} - \frac{1}{3}} \tag{8}$$

From Fig. 4 the condition for fibre lock-up may be defined as follows:

$$\text{HxV:} \qquad H_1 = \cos(\alpha-\beta)\cdot H_0/\cos\beta \quad \Rightarrow \quad \cos(\alpha-\beta) = C\cdot\cos\beta$$
$$\alpha = \beta + \text{Arccos}(C\cos\beta) \qquad \text{where } C = H_1/H_0 \tag{9}$$

3.3. Bounds for the lock-up angle and kink-band angle

It is obvious that the upper limit for the fibre rotation is 90°. From Eqs (3) and (9) it may be observed that $\partial\alpha/\partial\beta > 0$. Hence, the lower bound for α is obtained for $\beta = 0°$ and the upper bound for α is 90°, unless a value of β is given. Furthermore $\alpha \ge \beta + \text{Arccos}(C)$, i.e. $\beta \le \alpha - \text{Arccos}(C) \le \alpha/2$. Thus, the following bounds may be established for α and β:

$$\alpha_{\min} \le \alpha \le 90° \quad \text{where} \quad \alpha_{\min} = \text{Arccos}(C) \tag{10}$$

$$0° \le \beta \le \min\{90° - \alpha_{\min}, 45°\} \tag{11}$$

3.4. Predictions of the fibre lock-up angle

The lower bounds for the lock-up angle as functions of fibre volume fraction for the four different fibre arrays have been plotted in Fig. 5, together with some maximum fibre rotation angles measured by use of 3D micro-CT [13].

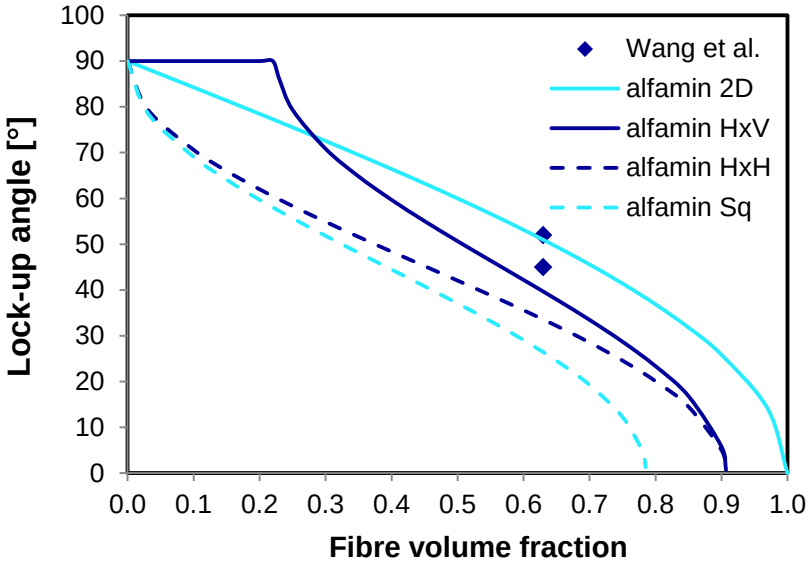

Figure 5. Lower bounds (assuming β=0) for the lock-up angle α vs v_f for the four fibre arrays.

4. Ply stiffness after lock-up

After lock-up the fibres will be in lateral contact, and the stiffness transverse to the fibres will be controlled by the contact of fibre cylinders. Reviews of relevant solutions are given in [14-15]. In the following analysis we neglect the minor stiffness contribution of the matrix between fibres after lock-up but it could easily be included, e.g. as parallel springs in a simplified micromechanics model.

4.1 Transverse stiffness with contacting fibres in parallel planes

In this case each fibre will be compressed vertically between two neighbouring fibres. The case is identical to the diametrical compression of a cylinder between two rigid flat surfaces, which was solved by Föppl (1907), as described in [15]. For a unit cell of width d+t an average transverse pressure p_T results in a radial load N_r per unit length of fibre, and a contact half-width b between the fibres. The resulting transverse compression δ_r of a fibre with radial stiffness Q_r is given by:

$$\delta_r = (4/\pi)\left[1/3 + \ln(d/b)\right] N_r/Q_r \quad \text{where} \tag{12}$$

$$b = \sqrt{(4/\pi)\, d\, N_r/Q_r} \qquad Q_r = E_r/(1-\nu_r^2) \qquad N_r = p_T(d+t)$$

The resulting transverse strain is obtained by dividing δ_r with the fibre diameter d

$$\varepsilon_T = \delta_r/d = (4/\pi)\left[1/3+\ln(d/b)\right](p_T/Q_r)(d+t)/d \tag{13}$$

The resulting transverse stiffness Q_T, Eq. (14), is obtained by dividing p_T with the transverse strain ε_T. The corresponding value of ψ for the different fibre arrays is given in Eq. (15).

$$Q_T = p_T/\varepsilon_T = Q_r\psi/\left[1/3+\ln(d/b)\right] \qquad \text{where} \quad d/b = \sqrt{\psi Q_r/p_T} \tag{14}$$

$$\text{Sq:} \qquad \psi = (\pi/4)d/(d+t) = \sqrt{v_f\pi/4}$$

$$\text{HxH:} \qquad \psi = (\pi/4)d/(d+t) = \sqrt{v_f\pi\sqrt{3}/8} \tag{15}$$

The influence of the transverse pressure p_T on the transverse stiffness Q_T after lock-up for glass and carbon fibres in a square fibre array is shown in Fig. 6. The behaviour is similar for other fibre arrays.

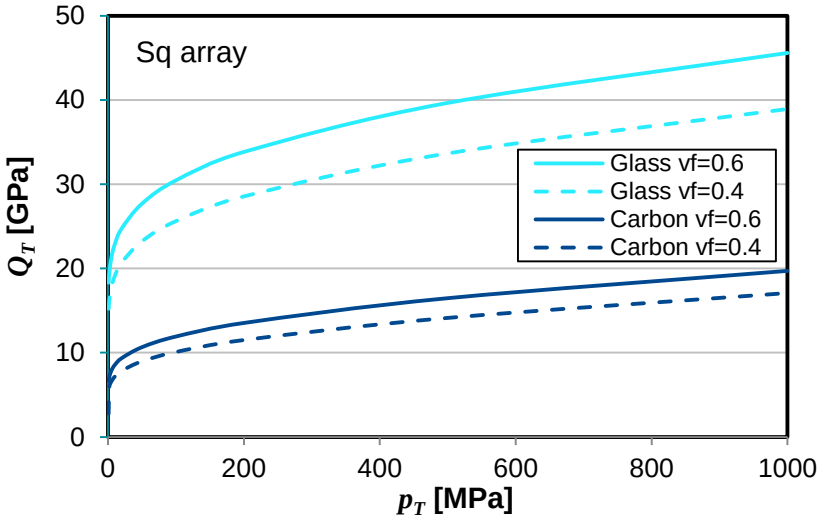

Figure 6. Transverse ply stiffness of kink band after fibre lock-up in a square fibre array (Sq).

4.2 Transverse stiffness with contacting fibres in intersecting planes

The geometry at fibre lock-up for the hexagonal array with vertical symmetry (HxV) with $v_f > \pi/(8\sqrt{3})$ is shown in Fig. 7. By use of Eqs (7) and (8) we obtain Eq. (16).

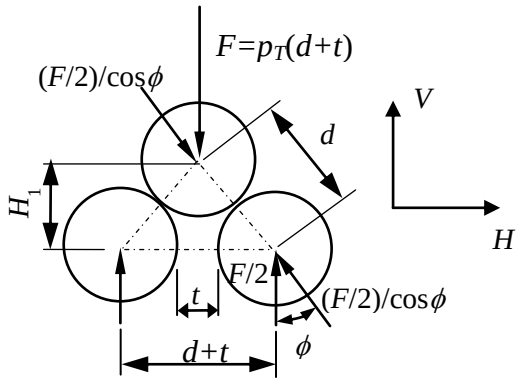

Figure 7. Geometry at fibre lock-up for hexagonal symmetry HxV

$$d/(d+t)=\sqrt{v_f\,2\sqrt{3}/\pi}\quad \cos\phi=H_1/d \quad \Rightarrow$$
$$H_1/(d+t)=\sqrt{d^2/(d+t)^2-1/4}=\sqrt{v_f\,2\sqrt{3}/\pi-1/4} \tag{16}$$

The vertical displacement due to transverse fibre compression is given by the following equation:

$$\delta_V=\delta_r\cos\phi=\frac{4p_V(d+t)/2}{\pi Q_r\cos\phi}\cos\phi\left[1/3+\ln(d/b)\right] \qquad b=\sqrt{\frac{4p_V(d+t)d}{\pi Q_r 2\cos\phi}}$$
$$\delta_V=\frac{2p_V(d+t)}{\pi Q_r}\left[1/3+\ln(d/b)\right] \qquad d/b=\sqrt{\frac{\pi Q_r d\cos\phi}{2p_V(d+t)}}=\sqrt{\frac{\pi Q_r H_1}{2p_V(d+t)}} \tag{17}$$

The resulting vertical strain is then given by Eq. (18). Finally the transverse stiffness, Eq. (19), is obtained by dividing the vertical pressure with the strain.

$$\varepsilon_V=\delta_V/H_1=\frac{2p_V(d+t)}{\pi Q_r H_1}\left[1/3+\ln(d/b)\right] \tag{18}$$

$$\text{HxV:} \qquad Q_T=p_V/\varepsilon_V=Q_r\psi/\left[1/3+\ln(d/b)\right] \qquad \text{where}$$
$$d/b=\sqrt{\psi Q_r/p_V} \qquad \text{and} \qquad \psi=(\pi/2)H_1/(d+t)=\sqrt{v_f\pi\sqrt{3}/2-\pi^2/16} \tag{19}$$

4.3 Stiffness of the kink band after fibre lock-up

The stiffness of the kink band in the original fibre direction ("1") is obtained using conventional transformation of the damaged stiffness coefficients Q_{ij}^d (Q_{ij} are the undamaged properties):

$$\bar{Q}_{11}^d=Q_{11}^d\cos^4\alpha+2\left(Q_{12}^d+Q_{66}^d\right)\cos^2\alpha\cdot\sin^2\alpha+Q_{22}^d\sin^4\alpha \tag{20}$$
$$\text{where} \quad Q_{11}^d=Q_{11} \qquad Q_{12}^d=Q_{12} \qquad Q_{66}^d=0 \qquad Q_{22}^d=Q_T$$

Here it has been assumed that the axial stiffness and transverse Poisson's ratio are unaffected in compression, while the shear stiffness after extensive shear microcracking is zero. In general the stiffness will be much lower than the initial stiffness prior to kinking, but the increase in the transverse stiffness Q_T after fibre lock-up contributes to a somewhat higher stiffness, particularly for glass fibres ($Q_r \approx 70$ GPa), which have a much higher transverse modulus than carbon fibres ($Q_r \approx 20$-25 GPa).

5. Discussion and conclusions

Lower bounds for the fibre lock-up angle α versus fibre volume fraction v_f have been obtained for 3D fibre arrays by assuming a zero kink band angle, i.e. $\beta=0$. Upper bounds for α could not be established as it increases monotonously with β, for which no expressions could be derived or found in the literature. Future work should focus on deriving suitable expressions for the kink band angle β.

The hexagonal fibre array is generally considered the most representative of real fibre composites. The lower bounds for the fibre-lock up angle predicted for the hexagonal arrays are also closest to the 3D micro-CT measurements by Wang et al. [13]. The lock-up angle for the HxH array is somewhat lower than for the HxV array, but it is likely that kinking allows some lateral movement of the fibres, which might allow the fibres to reconfigure to the HxV configuration.

It is interesting to note that the 2D model provides a higher value for the lock-up angle than the 3D fibre configurations, although the current predictions only provide lower bounds for the lock-up angle. This may indicate that the analytical 2D models available in the literature overestimate the lock-up angle and that 3D models are required to provide more reliable values. Furthermore, for large shear strains the assumptions of elastic behaviour clearly need to be replaced by assumptions of plastic deformation or shear microcracking in the matrix.

Acknowledgments

The funding for this research from the Swedish Energy Agency (Energimyndigheten) through project 34181-2 is gratefully acknowledged.

References

[1] C.R. Chaplin. Compressive fracture in unidirectional glass-reinforced plastics. *J Materials Sci*, 12:347-352, 1977.
[2] P.M. Moran, X.H. Liu, and C.F. Shih. Kink band formation and band broadening in fiber composites under compressive loading. *Acta Metall Mater*, 43:2943-2958, 1995.
[3] B. Budiansky, N.A. Fleck, and J.C. Amazigo. On kink-band propagation in fiber composites. *J Mech Phys Solids*, 46:1637-1653, 1998.
[4] M.A. Wadee, et al. Geometric modelling of kink banding in laminated structures. *Phil Trans R Soc A*, 370:1827–1849, 2012.
[5] R.A.E. Zidek, and C. Völlmecke. Analytical studies on the imperfection sensitivity and on the kink band inclination angle of unidirectional fiber composites. *Composites A*:64:177-184, 2014.
[6] S.P.H. Skovsgaard, and H. Myhre Jensen. Steady-state kink band propagation in layered materials. *J Appl Mech*, 85:061005-1-061005-11, 2018.
[7] R. Gutkin, et al. On the transition from shear-driven fibre compressive failure to fibre kinking in notched CFRP laminates under longitudinal compression. *Compos Sci Technol*, 70:1223–1231, 2010.
[8] R. Gutkin, S. Costa, and R. Olsson. A physically based model for kink-band growth and longitudinal crushing of composites under 3D stress states accounting for friction. *Compos Sci Technol*, 135:39-45, 2016.
[9] S. Costa, R. Gutkin, and R. Olsson R. Mesh objective implementation of a fibre kinking model for damage growth with friction. *Compos Struct*, 168:384–391, 2017.
[10] T.J. Vogler, S.-Y. Hsu, and S. Kyriakides. On the initiation and growth of kink bands in fiber composites. Part II: analysis. *Int J Solids Struct*, 38:2653-2682, 2001.
[11] C.S. Yerramalli, and A.M. Waas. The effect of fiber diameter on the compressive strength of composites - a 3D finite element based study. *Computer Modelling in Engineering & Science* (cmes), 6:1-16, 2004.
[12] M. Bishara, R. Rolfes, and O. Allix. Revealing complex aspects of compressive failure of polymer composites – Part I: Fiber kinking at microscale. *Compos Struct*, 169:105-115, 2016.
[13] Y. Wang, et al. X-ray computed tomography study of kink bands in unidirectional composites. *Compos Struct*, 160:917-924, 2017.
[14] B.N. Norden. On the compression of a cylinder in contact with a plane surface. *NBSIR 73-243*. National Bureau of Standards, US Department of Commerce, 1973.
[15] M.R. Hoeprich, and H. Zantopulos. Line contact deformation: a cylinder between two flat plates. *J Lubrication Technol*, 103:21-25, 1981.